THE JOURNAL OF BIOLOGICAL CHEMISTRY VOL. 284, NO. 37, pp. 24840–24847, September 11, 2009

Aryl-alcohol Oxidase Involved in Lignin Degradation

A MECHANISTIC STUDY BASED ON STEADY AND PRE-STEADY STATE KINETICS AND PRIMARY AND SOLVENT ISOTOPE EFFECTS WITH TWO ALCOHOL SUBSTRATES[*] [S]

Received for publication, April 22, 2009, and in revised form, July 1, 2009 Published, JBC Papers in Press, July 2, 2009, DOI 10.1074/jbc.M109.011593

Patricia Ferreira[‡§1], **Aitor Hernandez-Ortega**[‡2], **Beatriz Herguedas**[§], **Ángel T. Martínez**[‡3], **and Milagros Medina**[§4]

From the [‡]*Centro de Investigaciones Biológicas (CIB), Consejo Superior de Investigaciones Científicas (CSIC), E28040 Madrid and the* [§]*Departamento de Bioquímica y Biología Molecular y Celular, Facultad de Ciencias and Instituto de Biocomputación y Física de Sistemas Complejos, Universidad de Zaragoza, E-50009 Zaragoza, Spain*

Aryl-alcohol oxidase (AAO) is a FAD-containing enzyme in the GMC (glucose-methanol-choline oxidase) family of oxidoreductases. AAO participates in fungal degradation of lignin, a process of high ecological and biotechnological relevance, by providing the hydrogen peroxide required by ligninolytic peroxidases. In the *Pleurotus* species, this peroxide is generated in the redox cycling of *p*-anisaldehyde, an extracellular fungal metabolite. In addition to *p*-anisyl alcohol, the enzyme also oxidizes other polyunsaturated primary alcohols. Its reaction mechanism was investigated here using *p*-anisyl alcohol and 2,4-hexadien-1-ol as two AAO model substrates. Steady state kinetic parameters and enzyme-monitored turnover were consistent with a sequential mechanism in which O_2 reacts with reduced AAO before release of the aldehyde product. Pre-steady state analysis revealed that the AAO reductive half-reaction is essentially irreversible and rate limiting during catalysis. Substrate and solvent kinetic isotope effects under steady and pre-steady state conditions (the latter showing ~9-fold slower enzyme reduction when α-bideuterated substrates were used, and ~13-fold slower reduction when both substrate and solvent effects were simultaneously evaluated) revealed a synchronous mechanism in which hydride transfer from substrate α-carbon to FAD and proton abstraction from hydroxyl occur simultaneously. This significantly differs from the general mechanism proposed for other members of the GMC oxidoreductase family that implies hydride transfer from a previously stabilized substrate alkoxide.

Wood and other lignocellulosic materials are the main source of renewable materials in earth. White-rot basidiomycetes are essential contributors to carbon cycling in forest and other land ecosystems because of their ability to degrade lignocellulose to carbon dioxide and water. This ability confers to these fungi and their ligninolytic enzymes high interest in industrial processes, such as bioethanol production and paper pulp manufacturing, where the removal of lignin is a previous and essential step to use the cellulose present in plant biomass as a source for renewable fuels, chemicals, and materials (1).

Aryl-alcohol oxidase (AAO)[5] is an extracellular FAD-containing enzyme (2) that, in collaboration with myceliar aryl-alcohol dehydrogenases, participates in lignin degradation by some white-rot fungi, such as *Pleurotus* (and *Bjerkandera*) species, by generating hydrogen peroxide in the redox cycling of aromatic fungal metabolites, such as *p*-anisaldehyde (3, 4). Fungal high redox-potential peroxidases catalyze the oxidative degradation of lignin by this extracellular peroxide (5).

AAO was cloned for the first time in *Pleurotus eryngii* (6), a fungus of biotechnological interest because of its ability to degrade lignin selectively (7). The AAO amino acid sequence revealed moderate homology with glucose oxidase from *Aspergillus niger* (8), a flavoenzyme in the glucose-methanol-choline oxidases (GMC) oxidoreductase family. The reported molecular model of AAO (9), based on the glucose oxidase crystal structure (10), showed common features with the overall structural topology of bacterial choline oxidase and almond hydroxynitrile lyase (a lyase with oxidoreductase structure), as well as with other members of the GMC family; such as the extracellular flavoenzymes pyranose-2-oxidase and cellobiose dehydrogenase from white-rot basidiomycetes, and bacterial cholesterol oxidase (11–15). In particular, *P. eryngii* AAO conserves two histidine residues, His-502 and His-546 (supplemental Fig. S1), involved in catalysis in different members of this family (the second residue is an asparagine in some of them) (9).

Non-glycosylated *P. eryngii* AAO expressed in *Escherichia coli* (16) is used for further characterization studies. The enzyme catalyzes the oxidative dehydrogenation of unsaturated alcohols with a primary hydroxyl at Cα, exhibiting broad substrate specificity. In addition to benzyl alcohols, its active site also binds and oxidizes aliphatic polyunsaturated primary alcohols (such as 2,4-hexadien-1-ol), naphthyl, and cinnamyl alcohols, and shows low activity on some aromatic aldehydes (17). Methanol and other saturated alcohols are not AAO sub-

* This work was supported by the Spanish Projects BIO2005-03569, BIO2007-65890-C02-01, and BIO2008-01533, and the BIORENEW Project of the European Union (Contract NMP2-CT-2006-026456).

[S] The on-line version of this article (available at http://www.jbc.org) contains supplemental methods, Equations S1–S8, Table S1, and Figs. S1–S5.

[1] Supported by a Juan de la Cierva contract from the Spanish Ministry of Science and Innovation.

[2] Supported by a predoctoral contract from the Comunidad de Madrid.

[3] To whom correspondence may be addressed: CIB, CSIC, Ramiro de Maeztu 9, E-28040 Madrid, Spain. Tel.: 34-918373112; Fax: 34-915360432; E-mail: atmartinez@cib.csic.es.

[4] To whom correspondence may be addressed: Facultad de Ciencias, Universidad de Zaragoza, E-50009 Zaragoza, Spain. Tel.: 34-976762476; Fax: 34-976762123; E-mail: mmedina@unizar.es.

[5] The abbreviations used are: AAO, aryl-alcohol oxidase; GMC, glucose-methanol-choline oxidases; KIE, kinetic isotope effect.

strates, and the monounsaturated allyl alcohol is very slowly oxidized (2).

It is suggested that the AAO catalytic mechanism proceeds via electrophilic attack and direct transfer of a hydride to the flavin (17). A recent mutational study confirmed the strict requirement for catalysis of His-502 and His-546 located near the isoalloxazine ring of FAD (supplemental Fig. S1), as well as the involvement of two aromatic residues (18). Here we present the first study on the reaction mechanism of AAO in which substrate and solvent kinetic isotope effect (KIE), in combination with bisubstrate steady state and pre-steady state kinetic approaches, have been used to investigate the mechanism of polyunsaturated primary alcohol oxidation by AAO. Its natural substrate, *p*-anisyl alcohol, as well as a structurally different (non-aromatic) AAO substrate, 2,4-hexadien-1-ol, were chosen as two models for the different AAO alcohol substrates.

EXPERIMENTAL PROCEDURES

Chemicals—*p*-Anisyl alcohol, 2,4-hexadien-1-ol, *p*-anisic acid, 3-fluorobenzyl alcohol, sodium deuteroxide, and deuterium oxide (99.9%) were purchased from Sigma-Aldrich. *p*-[α-$^2H_2$]anisyl alcohol ([1,1-$^2H_2$]1-(4′-methoxyphenyl)-methanol) and [α-$^2H_2$]2,4-hexadien-1-ol ([1,1-$^2H_2$]2,4-hexadien-1-ol) were synthesized at the Instituto de Ciencia de Materiales de Aragón (CSIC-UZ, Zaragoza, Spain).

Production of the Recombinant Enzyme—Recombinant AAO of *P. eryngii* was obtained by *E. coli* expression of the mature AAO cDNA (GenBank™ AF064069) followed by *in vitro* activation in the presence of the cofactor and purification by ion-exchange chromatography (16).

Spectra and Steady State Kinetic Parameters—Absorption spectra and steady state kinetic analyses were performed in a Cary 100 Bio spectrophotometer. AAO concentrations were determined using $\epsilon_{463ox} = 11050\ M^{-1}\ cm^{-1}$ (16).

Steady state kinetic measurements were monitored spectrophotometrically by oxidation of the alcohols (*p*-anisyl alcohol or 2,4-hexadien-1-ol) to the corresponding aldehydes (17). Two-substrate steady state kinetic measurements were performed varying either the concentrations of the alcohol or O_2 as described under supplemental materials (see also supplemental Eqs. S1 and S2). The pH (4–9) dependence of AAO activity was studied at 25 °C with *p*-anisyl alcohol as substrate under different O_2 concentrations. Buffers used were 100 mM citrate phosphate for pH 4–7, and 100 mM pyrophosphate for pH 8–9.

Inhibition Studies—The K_d for the AAO complex with *p*-anisic acid was measured by titration of 16 μM AAO with *p*-anisic acid (0–1.24 mM) in 100 mM phosphate, pH 6, at 25 °C. The inhibition of AAO activity by *p*-anisic acid was studied at 25 °C, under atmospheric O_2 concentration, using veratryl alcohol as substrate. Measurements were carried out at different pH values (supplemental Eqs. S3–S5 were used). Buffers used were the above indicated for steady state kinetics.

Stopped-flow Kinetic Measurements—Experiments were carried out with an Applied Photophysics SX17.MV spectrophotometer interfaced with an Acorn computer. The SX18.MV and Xscan softwares were used for experiments using the single wavelength or photodiode array (350–700 nm) detectors, respectively.

TABLE 1

Kinetic parameters (of steady and pre-steady states) for AAO oxidation of *p*-anisyl alcohol and 2,4-hexadien-1-ol

Assays were performed in 100 mM phosphate, pH 6, at 12 °C.

	Steady state[a]			Pre-steady state[b]	
	k_{cat}	K_m^S	$K_m^{O_2}$	k_{red}	$K_{d[AAO:S]}$
	s^{-1}	μM	μM	s^{-1}	μM
p-Anisyl alcohol	129 ± 5	25 ± 3	348 ± 36	139 ± 16	26 ± 5
2,4-Hexadien-1-ol	161 ± 3	91 ± 5	232 ± 13	144 ± 2	62 ± 4

[a] Steady state constants were determined by varying the concentrations of both reducing substrates and O_2, and fitted to supplemental Eq. S1 that describes a ternary mechanism.

[b] Kinetic traces of AAO (FAD) reduction were fitted to supplemental Eq. S6.

For enzyme-monitored turnover experiments (19), equal volumes of air-saturated enzyme and substrate solutions were mixed, and evolution of the redox state of the flavin cofactor was monitored. Reductive half-reactions were studied under anaerobic conditions as described in the supplemental materials (see also supplemental Eqs. S6 and S7). Measurements were carried out in 100 mM phosphate, pH 6, at 12 °C.

Substrate and Solvent KIE—Steady state KIE experiments were performed in 100 mM phosphate under atmospheric O_2 (0.273 mM at 25 °C) as described above, but using bideuterated substrates (*p*-[α-$^2H_2$]anisyl alcohol and [α-$^2H_2$]2,4-hexadien-1-ol) and/or deuterated solvent. pH profiles for V_{max} and V_{max}/K_m KIE values were estimated in the pH 4–9 range. For assays in deuterated solvent, the reaction components were dissolved in deuterated 100 mM phosphate, pD 6. AAO was exhaustively dialyzed against the buffer to remove exchangeable protons. Pre-steady state substrate and solvent KIE for the AAO reductive half-reaction were analyzed at 12 °C under anaerobic conditions, as described above. The solvent viscosity effect on steady state parameters was measured as described under supplemental materials.

Data Analysis—Data analysis of the different measurements was carried out as described under supplemental data.

RESULTS

Steady State Alcohol Oxidation by AAO—The double reciprocal plots of *p*-anisyl alcohol and 2,4-hexadien-1-ol oxidation rates at different O_2 concentrations showed a series of lines converging at the left side of the *y* axis (supplemental Fig. S2). This suggests a sequential mechanism in which O_2 reacts with the reduced enzyme before release of the product takes place. According to this kinetic pattern, the best data fitting (supplemental Eq. S1) was consistent with a ternary complex mechanism. The steady-state kinetic parameters for both substrates are summarized in Table 1 (left).

AAO Inhibition with p-Anisic Acid—The strength of *p*-anisic acid binding on AAO, calculated from the perturbation in the cofactor spectrum upon titration with the inhibitor at pH 6 (Fig. 1, *inset*), resulted in a K_d value of 94 ± 3 μM, in agreement with the K_i (80 ± 2 μM) previously reported (17). Because the pK_a values of competitive inhibitors are expected to reflect intrinsic values (20), *p*-anisic acid inhibition was determined as a function of pH (Fig. 1). Data fitting (supplemental Eq. S2) indicated that binding of the inhibitor is enhanced by protonation of a group with a pK_a of 7.5 ± 0.1.

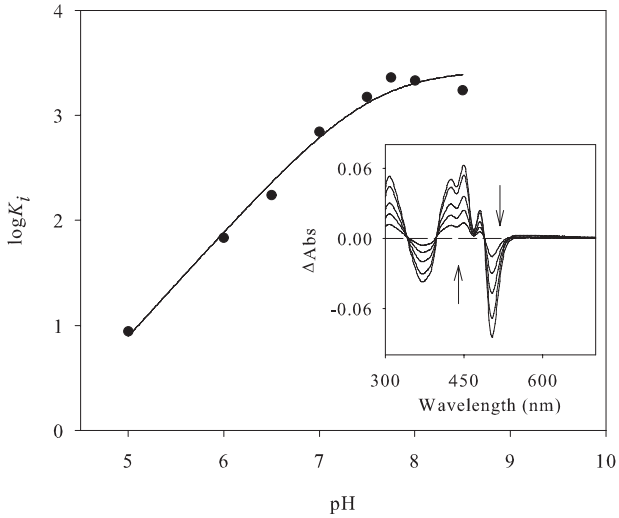

FIGURE 1. **AAO inhibition with *p*-anisic acid.** pH dependence of the constant of AAO inhibition by *p*-anisic acid. AAO activity inhibition was measured with veratryl alcohol as substrate in the presence of *p*-anisic acid in air-saturated buffer at 25 °C. The *inset* shows the difference spectra upon *p*-anisic acid binding to AAO. The titration was performed at 25 °C in 100 mM phosphate, pH 6. The curves shown are the difference spectra after addition of 18, 48, 106, 278, and 698 μM *p*-anisic acid (in the order indicated by the *arrows*).

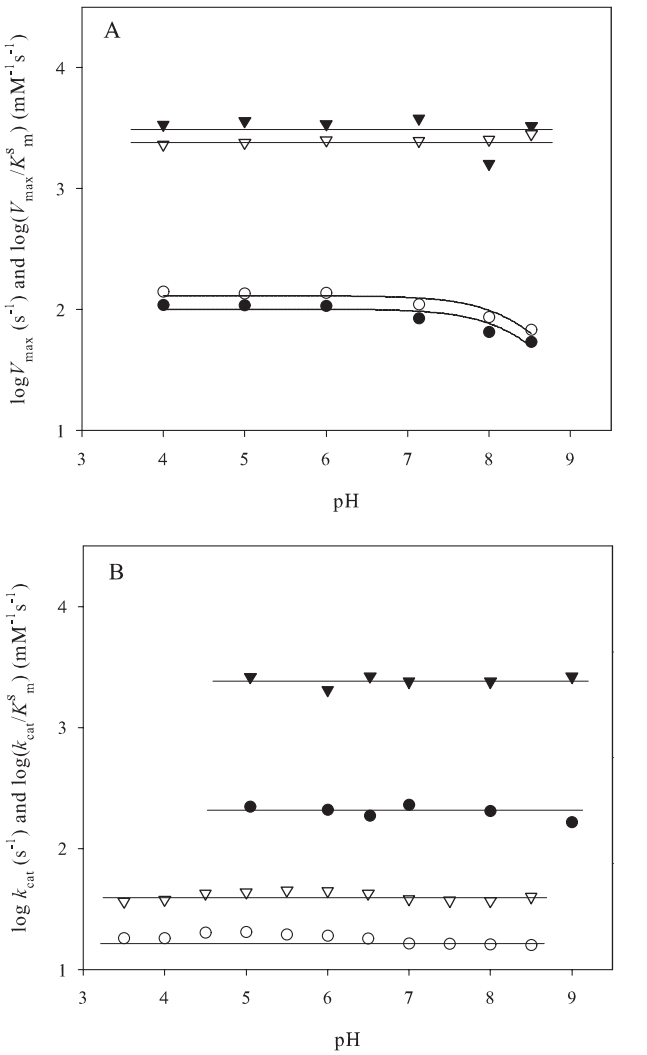

FIGURE 2. **pH dependence of AAO steady state parameters for several substrates.** *A*, pH dependence of the V_{max} and V_{max}/K^S_m for *p*-anisyl alcohol (● and ▼, respectively) and 2,4-hexadien-1-ol (○ and ▽, respectively) in air-saturated buffer. *B*, pH dependence of the k_{cat} and k_{cat}/K^S_m values for *p*-anisyl (● and ▼, respectively) and 3-fluorobenzyl alcohol (○ and ▽, respectively) under saturating O_2 concentrations (air and O_2-saturated buffer for 3-fluorobenzyl alcohol and *p*-anisyl alcohol, respectively). All reactions were performed at 25 °C.

The pH Dependence of AAO Activity—pH dependence of the AAO steady state kinetic parameters for oxidation of *p*-anisyl alcohol and 2,4-hexadien-1-ol was first determined under atmospheric O_2. As shown in Fig. 2*A*, the V_{max} values (*circles*) were independent from pH 4 to 7, but decreased at greater pH values. Recombinant AAO is unstable at a pH beyond 9; therefore the V_{max} pH profile suggests that a group with a p$K_a \geq 8.5$ must be protonated for catalysis. In contrast, the AAO catalytic efficiency (*triangles*) was pH-independent, suggesting a decrease in K^S_m (Fig. 2*A*).

A second set of experiments varying simultaneously the concentrations of *p*-anisyl alcohol and O_2 was carried out. The k_{cat}, k_{cat}/K^S_m and $k_{cat}/K^{O_2}_m$ values obtained after data fitting (to supplemental Eq. S1) were independent of pH at saturating concentrations of both AAO oxidizing and reducing substrates, as shown in Fig. 2*B* (*black symbols*) for *p*-anisyl alcohol oxidation.

The pH dependence of AAO activity was also analyzed with a substrate presenting considerably slower reactivity, 3-fluorobenzyl alcohol (17). It was chosen expecting that chemical steps (rather than substrate binding and product release) would be rate limiting, thus allowing determination of true pK_a values in AAO catalysis. Because the AAO $K^{O_2}_m$ for 3-fluorobenzyl alcohol is 17 μM, reactions under atmospheric O_2 result in an AAO saturating concentration for this substrate, and the pH dependence study was only performed under the these conditions. In Fig. 2*B*, a lack of pH dependence for 3-fluorobenzyl alcohol oxidation (*white symbols*) was observed. Therefore, under O_2 saturation, AAO shows no pH dependence of k_{cat} or catalytic efficiency for the substrates analyzed.

Redox State of the Cofactor during Catalysis—To identify the redox state of the FAD cofactor during catalysis, AAO was mixed in the stopped-flow instrument with saturating concentrations of *p*-anisyl alcohol and 2,4-hexadien-1-ol under atmospheric O_2 (Fig. 3 and supplemental Fig. S3, respectively). A fast decrease in absorbance was observed within the first millisec-

onds after mixing (instrumental dead time), indicating reduction of the FAD. However, shortly after this initial decay, a lag period is observed. This suggests a steady state situation with competition between reduction of the flavin by the substrate and reoxidation by O_2. During turnover conditions, the fraction of oxidized enzyme remained around 75–70% of the total (as shown in the insets). This steady state period was short, and subsequent reduction of the FAD cofactor to its hydroquinone form was observed. Therefore, reduced AAO only accumulated after depletion of the O_2 present in solution, suggesting that the reductive half-reaction limits AAO catalysis.

On the other hand, the spectral evolution during *p*-anisyl alcohol oxidation suggests formation of a charge-transfer complex (Fig. 3). Additionally, a displacement of the position of the flavin band-I from 463 to 458 nm, and a better resolution of the shoulder at 474 nm, were observed for both substrates already in the first spectrum after mixing. These changes are in agree-

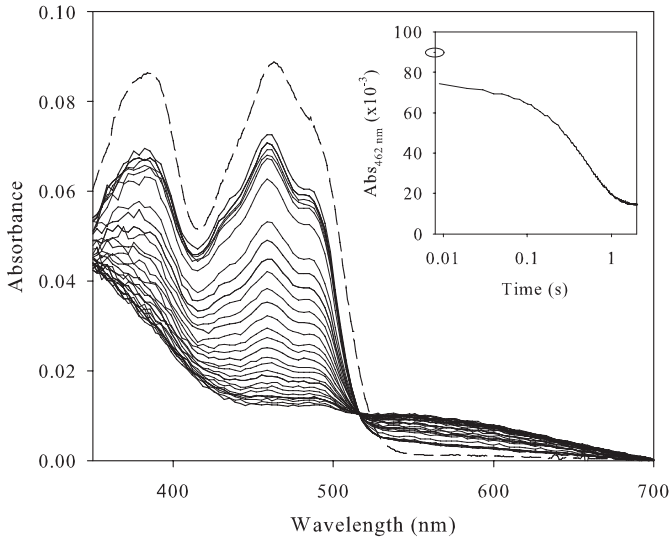

FIGURE 3. **Time-dependent spectral changes during AAO turnover with *p*-anisyl alcohol.** An aerobic solution of AAO (9 μM) was reacted in the stopped-flow instrument with 1 mM *p*-anisyl alcohol. The oxidized AAO spectrum before mixing is indicated by a *dashed line*, the first spectrum was recorded 0.009 s after mixing, in the 0.009–0.050 s range spectra are shown each 10 ms, and thereafter each 50 ms. The *inset* shows the course of the reaction monitored at 462 nm (logarithmic time scale). A *closed circle* indicates the initial absorbance of oxidized AAO. Measurements were carried out in 100 mM phosphate, pH 6, at 20 °C.

ment with those observed during titration with *p*-anisic acid (Fig. 1).

Reductive Half-reaction—Pre-steady state reduction of oxidized AAO by *p*-anisyl and 2,4-hexadien-1-ol was analyzed under anaerobic conditions (Fig. 4 and supplemental Fig. S4, respectively). The spectra obtained indicated full reduction of AAO by both alcohols without the appearance of any FAD semiquinone intermediate. Global analysis of the spectral evolution best fit to a three step model. The first process (A → B) was fast (over 100 s^{-1} for both alcohol substrates) and accounted for more than 80% of the amplitude of the reaction. The second process (B → C) was concentration-independent, and too slow (3–5 s^{-1}) to account for the turnover. Probably it has no catalytic relevance and, because it was not observed in the presence of O_2 (Fig. 3), might be related to slow product release in the absence of the second substrate. Noticeably, the absence of O_2 also prevented the displacement of the flavin band-I described above and the formation of the charge-transfer complex species.

k_{obs} values at different substrate concentrations were determined from single kinetic traces monitored at 460 nm to follow FAD reduction by *p*-anisyl alcohol and 2,4-hexadien-1-ol (bottom part of Fig. 4 and supplemental Fig. S4, respectively). The observed rates for the fast process (k_{obs1}) obeyed a Michaelis-Menten kinetic behavior. Data fits (to supplemental Eqs. S6 and S7) indicated insignificant k_{rev} values, in agreement with the photodiode-array analysis. Therefore, an essentially irreversible reduction of the flavin occurs during AAO catalysis with both substrates. The K_d and reduction rate (k_{red}) values derived from this analysis are shown in Table 1 (right). They are in agreement with the above-reported K_m^S and k_{cat}, indicating that the reductive half-reaction must be the rate-limiting step in AAO catalysis.

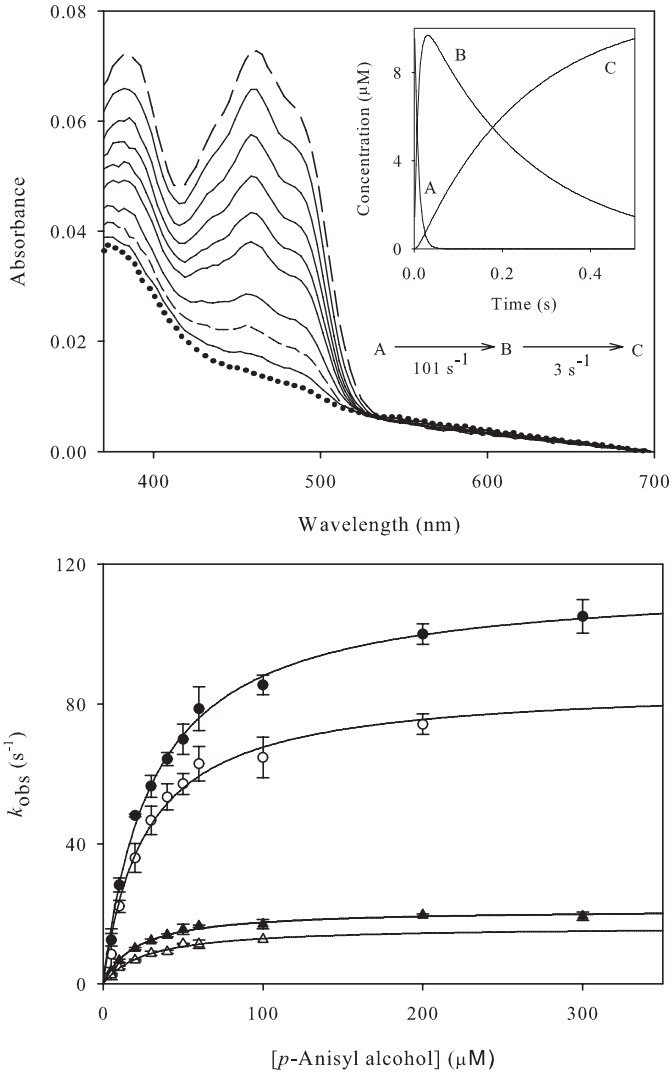

FIGURE 4. **Reductive half-reaction of AAO with *p*-anisyl alcohol.** *Top*, spectral changes observed upon anaerobic mixing of 8 μM AAO with 500 μM *p*-anisyl alcohol. Spectra at 1, 4, 6, 9, 12, 15, 22, 32, 93, and 255 ms after mixing are shown. The *inset* shows the simulated concentration dependence of the three spectral species obtained after globally fitting the experimental data to a three step model: A→B→C. Species A (*long dashed line*), B (*short dashed line*), and C (*dotted line*) are indicated in the main panel. They are spectral species, reflecting a distribution of enzyme intermediates at a certain point along the reaction and do not necessarily represent a single distinct enzyme intermediate. *Bottom*, dependence of the AAO reduction observed rates on the concentrations of *p*-anisyl alcohol (and its α-bideuterated analog) in water and deuterium oxide. Experiments performed with α-protiated substrates in water (●), α-protiated substrates in deuterium oxide (○), α-bideuterated substrates in water (▲), and α-bideuterated substrates in deuterium oxide (△). Data were fitted to supplemental Eq. S6. Assays were carried out in a stopped-flow spectrophotometer at 12 °C.

Substrate and Solvent KIE—Deuterium substitutions were used to further investigate if a hydride transfer mechanism leads to the AAO reductive half-reaction. Steady state parameters were determined using the α-bideuterated alcohol substrates (*p*-[α-$^2H_2$]anisyl alcohol and [α-$^2H_2$]2,4-hexadien-1-ol) under air-saturation conditions (supplemental Table S1, left). The turnover rates for these compounds (in water or deuterium oxide) revealed a significant substrate KIE, with V_{max} decreasing by a factor of ~5, and efficiency decreasing by 3.7–12.1-fold, at pH 6 (Table 2), suggesting that the breakdown of the alcohol Cα-H/D bond is limiting the rate of flavin reduction and, there-

TABLE 2

Substrate, solvent, and multiple KIE on AAO steady-state constants for *p*-anisyl alcohol and 2,4-hexadien-1-ol oxidation

Assays were performed in normal and deuterated 100 mM phosphate, pH 6 (at 25 °C, under air saturation conditions) using the α-protiated and α-bideuterated alcohol substrates. Different KIE estimated: ^{D}k, substrate KIE in water (i.e. k for α-protiated substrate in water/k for α-bideuterated substrate in water); $^{D}k_{(D_2O)}$, substrate KIE in D_2O (i.e. k for α-protiated substrate in deuterium oxide/k for α-bideuterated substrate in D_2O); ^{D_2O}k, solvent KIE using α-protiated substrate (i.e. k for α-protiated substrate in water/k for α-protiated substrate in D_2O); $^{D_2O}k_{(D)}$, solvent KIE using α-bideuterated substrate (i.e. k for α-bideuterated substrate in water/k for α-bideuterated substrate in D_2O); $^{D,D_2O}k$, simultaneous substrate and solvent KIE (i.e. k for α-protiated substrate in water/k for α-bideuterated substrate in D_2O). The experimental kinetic parameters for V_{max} and K_m used to calculate the KIE are reported in supplemental Table S1.

	p-Anisyl alcohol	2,4-Hexadien-1-ol
Substrate KIE		
$^{D}V_{max}$	5.41 ± 0.14	5.59 ± 0.14
$^{D}(V_{max}/K_m)$	3.71 ± 0.25	9.16 ± 1.08
$^{D}V_{max(D_2O)}$	5.22 ± 0.34	5.57 ± 0.10
$^{D}(V_{max}/K_m)_{(D_2O)}$	5.32 ± 0.65	12.10 ± 0.80
Solvent KIE		
$^{D_2O}V_{max}$	1.35 ± 0.06	1.25 ± 0.03
$^{D_2O}(V_{max}/K_m)$	1.15 ± 0.11	1.26 ± 0.11
$^{D_2O}V_{max(D)}$	1.30 ± 0.07	1.25 ± 0.02
$^{D_2O}(V_{max}/K_m)_{(D)}$	1.65 ± 0.17	1.66 ± 0.17
Multiple KIE		
$^{D,D_2O}V_{max}$	7.03 ± 0.38	6.98 ± 0.15
$^{D,D_2O}(V_{max}/K_m)$	6.12 ± 0.58	15.20 ± 1.10

fore, of the overall catalysis. Whereas the substrate KIE on V_{max} was not significantly different in water and deuterium oxide, stronger effects were observed on the efficiency of reactions in deuterium oxide (the $^{D}(V_{max}/K_m)_{(D_2O)}$ values for both alcohol substrates being 1.3–1.4-fold higher than the $^{D}(V_{max}/K_m)$ values).

The observed $^{D}V_{max}$ for alcohol oxidation by AAO resulted in pH dependence (Fig. 5*A*), increasing with protonation of a group with pK_a of 7.1 ± 0.2 and 7.4 ± 0.2 for *p*-anisyl and 2,4-hexadien-1-ol, respectively. These values are in the range of those for *p*-anisic acid inhibition (Fig. 1) and one unit lower than found for V_{max} on both substrates (Fig. 2*A*). In contrast, $^{D}(V_{max}/K_m)$ was pH-independent (Fig. 5*B*) showing average KIE values of 4.1 ± 0.3 and 9.4 ± 0.9 for *p*-anisyl and 2,4-hexadien-1-ol, respectively, in agreement with the lack of pH effect on AAO catalytic efficiency (Fig. 2*A*). Comparison of the steady state KIE values for both substrates at pH 6 (Table 2) showed that the *p*-anisyl alcohol $^{D}V_{max}$ was significantly larger than the $^{D}(V_{max}/K_m)$, suggesting that external commitments to catalysis partially mask the KIE with this substrate.

To probe the timing of the kinetic steps involving solvent exchangeable protons, such as the cleavage of the substrate OH bond (and alkoxide formation) during the reductive half-reaction, steady state kinetic parameters were also investigated at 25 °C (pH 6) using deuterated buffer (supplemental Table S1, left), and similar solvent effects were observed at 12 °C. In all cases, the solvent KIE observed (Table 2) was much lower than the substrate KIE described above. A solvent effect on $^{D_2O}V_{max}$ (1.25–1.35) was observed for both *p*-anisyl and 2,4-hexadien-1-ol, which was independent of their isotopic composition ($^{D_2O}(V_{max(D)})$) values of 1.25–1.30). Despite $^{D_2O}(V_{max}/K_m)$ values for both substrates were scarcely different from unity, a larger effect was observed when KIE was measured with deuterated substrates ($^{D_2O}(V_{max}/K_m)_{(D)}$) of 1.5–1.6) confirming the solvent effect. Moreover, a multiple KIE was observed (Table 2),

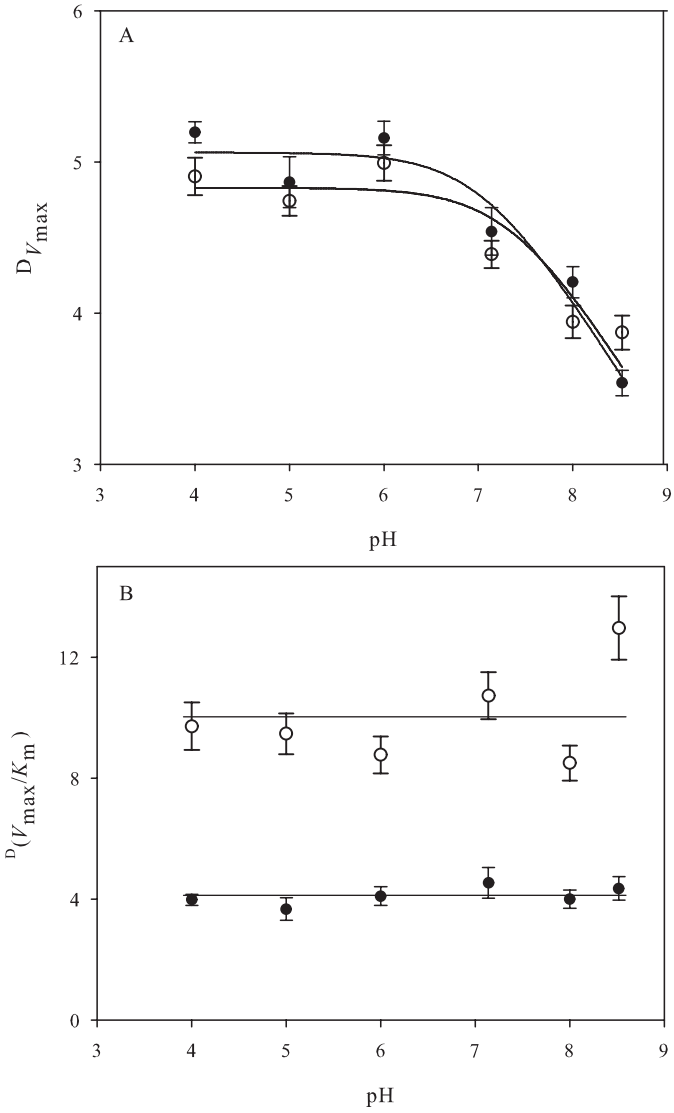

FIGURE 5. **pH dependence of the observed KIE for AAO steady state kinetic parameters.** pH dependence of $^{D}V_{max}$ (*A*) and $^{D}(V_{max}/K_m)$ (*B*) for [α-$^{2}H_2$]*p*-anisyl (●) and [α-$^{2}H_2$]2,4-hexadien-1-ol (○) oxidation by AAO are shown. Initial rates were determined with α-protiated and α-bideuterated substrates in 100 mM (protiated) phosphate, pH 4–8.5, at 25 °C under atmospheric O_2. Traces in *A* are the fit of data to supplemental Eq. S2.

being equal or higher to the product of the substrate and solvent KIE for V_{max} and V_{max}/K_m on both substrates.

The use of deuterium oxide increases the viscosity of the reaction medium (~23% with regard to water, at 25 °C). This could affect the rate of diffusion-limited steps, such as enzyme-substrate complex formation and product dissociation. The possible effect of viscosity on *p*-anisyl alcohol oxidation was investigated with increasing glycerol concentrations. No significant viscosity effects on V_{max} and V_{max}/K_m were observed (supplemental Fig. S5), enabling us to discard any viscosity-sensitive step in the removal of the alcohol hydroxyl proton by AAO.

The KIE studies were completed by calculations of pre-steady state substrate and solvent parameters for the reductive half-reaction using the two deuterated alcohol substrates under anaerobic conditions (pH 6) (supplemental Table S1, right). When mixing AAO with *p*-[α-$^{2}H_2$]anisyl alcohol or [α-$^{2}H_2$]2,4-

TABLE 3

Substrate, solvent, and multiple KIE on AAO presteady-state k_{red} by α-bideuterated *p*-anisyl alcohol and 2,4-hexadien-1-ol

Assays were performed in 100 mM phosphate, pH 6, at 12 °C, under anaerobic conditions. For the different KIE estimated, see Table 2 footnote.

	p-Anisyl alcohol	2,4-Hexadien-1-ol
Substrate KIE		
$^{D}k_{red}$	8.98 ± 0.82	8.93 ± 0.17
$^{D}k_{red(D_2O)}$	9.49 ± 0.36	9.41 ± 0.20
Solvent KIE		
$^{D_2O}k_{red}$	1.42 ± 0.10	1.33 ± 0.02
$^{D_2O}k_{red(D)}$	1.50 ± 0.10	1.41 ± 0.04
Multiple KIE		
$^{D,D_2O}k_{red}$	13.50 ± 0.90	12.50 ± 0.30

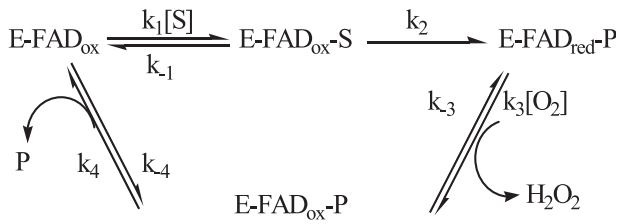

SCHEME 1

hexadien-1-ol, a complete irreversible reduction of the flavin was observed without detection of any intermediate semiquinone (not shown). For both α-bideuterated substrates, the $^{D}k_{red}$ was ~8.9, with nonsignificantly different $^{D}k_{red(D_2O)}$ values (Table 3). Moreover, a slight but significant solvent KIE was detected on $^{D_2O}k_{red}$ (1.3–1.4), apparently being independent of the substrate (nonsignificantly different $^{D_2O}k_{red(D)}$ values). Finally, the multiple substrate and solvent KIE on k_{red} resulted in the product of $^{D}k_{red}$ by $^{D_2O}k_{red}$ with $^{D,D_2O}k_{red}$ values around 13.5 and 12.5 for *p*-anisyl alcohol and 2,4-hexadien-1-ol, respectively. The KIE results are in agreement with a concerted mechanism for removal of the hydroxyl proton and hydride transfer to the flavin in AAO.

DISCUSSION

The AAO steady state kinetic parameters, obtained by varying both O_2 and alcohol substrate concentrations, are consistent with a ternary complex mechanism (Scheme 1) with O_2 reacting with the reduced enzyme before release of the aldehyde product.

Therefore, AAO appears to follow a similar sequential mechanism with regard to choline oxidase, a GMC oxidoreductase oxidizing alcohol substrates to the corresponding aldehydes and acids (17, 21), while a ping-pong mechanism appears to apply for glucose oxidase (19). Another flavoenzyme exhibiting a sequential mechanism is vanillyl alcohol oxidase (22), belonging to a family different of that from GMC oxidoreductases.

AAO shows high reactivity toward O_2 (3.7×10^5 and 7.0×10^5 M^{-1} s^{-1} in *p*-anisyl alcohol and 2,4-hexadien-1-ol oxidations, respectively) also described for glucose oxidase and vanillyl-alcohol oxidase (22, 23). In these two enzymes reorganization of the active site is related to reduced flavin activation for its reaction with O_2. Thus, glucose oxidase has been shown to enhance O_2 reactivity through protonation of a conserved histidine (His-516 of the *A. niger* enzyme) that has been related to a pK_a ~8 (23). Because this histidine is strictly conserved in GMC oxidoreductases, its involvement in the common reaction to all of them (*i.e.* the oxidative half-reaction) has been suggested (24). In contrast to that found for glucose oxidase, an effect of pH could not be detected in AAO $k_{cat}/K_m^{O_2}$, and the same has been reported for choline oxidase (25). Similar pK_a values have been found for substrate oxidation efficiencies of methanol oxidase (8.3 using benzyl alcohol) and choline oxidase (7.6 using choline) and assigned to histidines homologous to the above glucose oxidase one (His-568 of *Candida boidinii* methanol oxidase, and His-466 of *Arthrobacter globiformis* choline oxidase), which in this case should be unprotonated for catalysis suggesting its implication in substrate alkoxide formation (26–29).

We failed to detect any pH dependence of the AAO steady state parameters under saturating O_2 and *p*-anisyl concentrations, even when a less efficient substrate (Fig. 2*B*) was used to avoid possible external commitments to catalysis. However, a slight pH effect on AAO V_{max} was found under non-saturating O_2 concentration, suggesting that a residue with pK_a ~8.5 should be protonated for maximal turnover. Similar pH dependence has been described for veratryl alcohol oxidation by AAO expressed in *Emericella nidulans* (17) and for *p*-anisyl alcohol oxidation by the AAO from a different basidiomycete (30), as well as for oxidation of their respective substrates by cellobiose dehydrogenase and cholesterol oxidase (31, 32).

Interestingly, atomic resolution characterization of the *Streptomyces* sp. cholesterol oxidase as a function of pH, revealed that its conserved His-447 is in the singly protonated form in the pH range 4.5–7.3 (maximal turnover conditions), converting to the anionic imidazolate at pH 9 (15, 33). This residue is homologous to His-502 of *P. eryngii* AAO, and His-689 of *Phanerochaete chrysosporium* cellobiose dehydrogenase (18) (as well as to the glucose oxidase, methanol oxidase and choline oxidase conserved histidines mentioned above). The theoretically predicted pK_{a1} and pK_{a2} values for some of these histidines (34) also suggest a depression of both pK_a by the protein environment. Thus, the turnover dependence on pH in AAO, and some other GMC oxidoreductases, might be in agreement with the presence of a neutral singly protonated histidine (in the pH range 4–7) playing a role in catalysis. If this is the case, the V_{max} decrease at higher pH values could be related to deprotonation of conserved His-502 or His-546 (9) to its imidazolate form, negatively affecting AAO catalysis as proposed for cholesterol oxidase (33).

Alcohol oxidation by AAO requires the removal of a proton from the substrate hydroxyl and a formal hydride from its Cα position. Primary deuterium KIE was used to probe the status of the CH bond break, whereas solvent KIE can probe that of the OH bond. The similar $^{D}(V_{max}/K_m)$ and $^{D}k_{red}$ values found for 2,4-hexadien-1-ol oxidation are consistent with cleavage of the CH bond being not masked by other kinetics steps (belonging either to the reductive half-reaction or the overall turnover) and with the absence of any forward or reverse commitment to catalysis. Therefore, the KIE on the rate of flavin reduction ($^{D}k_{red}$) should be a direct measure of $^{D}k_2$, which is the magnitude expected for the intrinsic KIE. However, in AAO oxidation of *p*-anisyl alcohol the $^{D}(V_{max}/K_m)$ value obtained was lower than those of $^{D}V_{max}$ and $^{D}k_{red}$, and the cleavage of the CH bond does not appear to be the only rate-limiting step for catalysis.

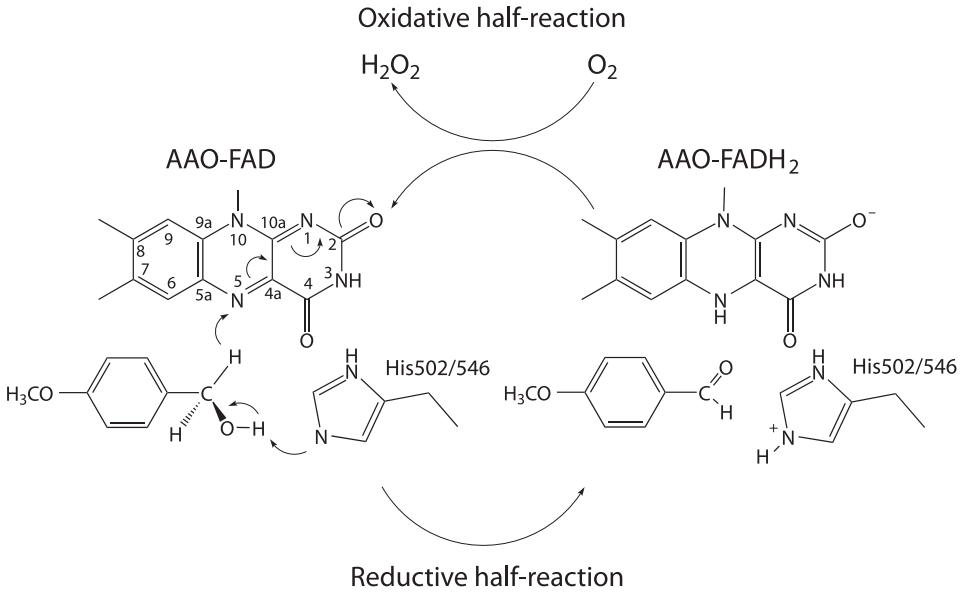

FIGURE 6. **Scheme for the AAO catalytic mechanism.** In the reductive half-reaction, oxidation of the alcohol substrate (in this case *p*-anisyl alcohol) would include simultaneous formation of the alkoxyde assisted by a catalytic base (His-502 or His-546 receiving the proton) and hydride transfer to the flavin N5. In the oxidative half-reaction, molecular oxygen returns flavin to its normal oxidized state, and the hydrogen peroxide required for lignin degradation is formed.

Stronger masking of bond cleavage has been found for cholesterol oxidase and glucose oxidase, with the reported KIE (around 2–3) significantly lower than their intrinsic values (32, 35, 36), whereas large substrate KIE values have been found for choline oxidase (27, 37). The complexities described made difficult an unambiguous determination of the catalytic mechanisms of the two former oxidases, while that of choline oxidase has been investigated during recent years as a model flavooxidase (38). In the mechanism proposed for AAO (Scheme 1), the observed complexity for *p*-anisyl alcohol oxidation must be due to the forward commitment to catalysis (k_2/k_{-1}) (see supplemental Eq. S8). Because AAO flavin reduction is rate limiting (and nearly irreversible) and AAO affinity for O_2 ($K_m^{O_2}$ of 275 μM) (39) is similar to the O_2 concentration under atmospheric conditions at 25 °C, a negligible reverse commitment to catalysis ($k_{-2}/k_3[O_2]$) is expected.

Regarding the status of the OH bond, a solvent KIE slightly larger than unity was observed on steady state parameters ($^{D_2O}V_{max}$, $^{D_2O}(V_{max}/K_m)$), whereas no viscosity contribution to such solvent KIE was observed. The increases of $^{D_2O}(V_{max}/K_m)_{(D)}$ and particularly the simultaneous substrate and solvent effects revealed by $^{D,D_2O}V_{max}$ and $^{D,D_2O}(V_{max}/K_m)$ (compared with $^{D}V_{max}$ and $^{D}(V_{max}/K_m)$ suggest that the solvent KIE must arise from substrate oxidation. These results differ substantially from those reported for other GMC oxidoreductases (such as glucose oxidase, cholesterol oxidase, and choline oxidase) where no solvent KIE has been detected upon substrate oxidation (32, 35–38).

Pre-steady state kinetic methods were additionally used to measure the substrate and solvent KIE on the reductive rate constant, k_{red} (k_2, Scheme 1), for *p*-anisyl alcohol and 2,4-hexadien-1-ol oxidations, without interference from other catalytic steps. The large KIE on k_{red} (~9) by both substrates permits us to establish that breaking of the CH bond occurs in the rate-limiting transition state for flavin reduction. These results, together with the multiple KIE observed with both substrates ($^{D,D_2O}k_{red}$ ~13), are consistent with a concerted hydride transfer mechanism in which both the proton removed from the hydroxyl group and the hydride being transferred to the flavin are concomitantly in flight in the transition state. Such a hydride transfer mechanism with simultaneous activation by a catalytic base (Fig. 6) is supported by the structural model of AAO that suggest the substrate CH bond to be cleaved is placed in front of the N5 position of the isoalloxazine ring, and close to the histidine residue/s contributing to the OH bond cleavage (see supplemental Fig. S1).

Substrate and solvent KIE studies on other members of the GMC oxidoreductase family have reported an asynchronous hydride transfer mechanism, in which the OH bond cleavage precedes the CH bond cleavage (20, 26). In fact, in choline oxidase the rate of proton abstraction is suggested to be significantly faster than the hydride transfer. Conserved histidine residues have been proposed to act as catalytic bases in the former reaction in different GMC oxidoreductases (26, 31, 32, 38, 40). In choline oxidase, conserved His-466 has been shown to contribute to stabilize the substrate alkoxide, as well as the sulfite adduct, instead of acting as the catalytic base (28). The synchronous mechanism here depicted for AAO discards stabilization of the alkoxide species during catalysis. This, together with the fact that this enzyme also fails in stabilizing a flavin adduct with sulfite (17), suggest that AAO does not stabilize intermediate interactions in its active site during catalysis, as found for other GMC oxidoreductases (41–43). Additionally, the large $^{D}k_{red}$ value also rules out a radical mechanism for AAO catalysis, since the observed decrease in k_{red} should result in a significant stabilization of any intermediate, as a semiquinone. This is in agreement with previous studies showing that AAO does not thermodynamically stabilize a flavin semiquinone radical (17). This characteristic of AAO, as well as its inability to form a covalent adduct with sulfite, are unexpected since both properties are typical of most oxidases (44).

In summary, the kinetic data here presented for AAO are consistent with a mechanism involving formation of the Michaelis-Menten complex, flavin reduction by substrate oxidation and, reoxidation of the reduced enzyme by O_2 with the concomitant release of the product. The reductive half-reaction is the rate-limiting step during AAO catalysis with both *p*-anisyl alcohol and 2,4-hexadien-1-ol. Moreover, the reductive half-reaction is consistent with a synchronous mechanism in which the OH and CH bond cleavages are in flight in the transition state, as shown by isotope effects. Therefore, AAO

catalysis appears as an exception in alcohol oxidation by GMC oxidoreductases, where a general asynchronous mechanism has been proposed (38).

REFERENCES

1. Martínez, A. T., Speranza, M., Ruiz-Dueñas, F. J., Ferreira, P., Camarero, S., Guillén, F., Martínez, M. J., Gutiérrez, A., and del Río, J. C. (2005) *Int. Microbiol.* **8,** 195–204
2. Guillén, F., Martínez, A. T., and Martínez, M. J. (1992) *Eur. J. Biochem.* **209,** 603–611
3. Gutiérrez, A., Caramelo, L., Prieto, A., Martínez, M. J., and Martínez, A. T. (1994) *Appl. Environ. Microbiol.* **60,** 1783–1788
4. Guillén, F., and Evans, C. S. (1994) *Appl. Environ. Microbiol.* **60,** 2811–2817
5. Ruiz-Dueñas, F. J., and Martínez, A. T. (2009) *Microbial Biotechnol.* **2,** 164–177
6. Varela, E., Martínez, A. T., and Martínez, M. J. (1999) *Biochem. J.* **341,** 113–117
7. Martínez, A. T., Camarero, S., Guillén, F., Gutiérrez, A., Muñoz, C., Varela, E., Martínez, M. J., Barrasa, J. M., Ruel, K., and Pelayo, M. (1994) *FEMS Microbiol. Rev.* **13,** 265–274
8. Frederick, K. R., Tung, J., Emerick, R. S., Masiarz, F. R., Chamberlain, S. H., Vasavada, A., Rosenberg, S., Chakraborty, S., and Schopter, L. M. (1990) *J. Biol. Chem.* **265,** 3793–3802
9. Varela, E., Jesús, Martínez, M., and Martínez, A. T. (2000) *Biochim. Biophys. Acta* **1481,** 202–208
10. Hecht, H. J., Kalisz, H. M., Hendle, J., Schmid, R. D., and Schomburg, D. (1993) *J. Mol. Biol.* **229,** 153–172
11. Quaye, O., Lountos, G. T., Fan, F., Orville, A. M., and Gadda, G. (2008) *Biochemistry* **47,** 243–256
12. Dreveny, I., Gruber, K., Glieder, A., Thompson, A., and Kratky, C. (2001) *Structure* **9,** 803–815
13. Bannwarth, M., Bastian, S., Heckmann-Pohl, D., Giffhorn, F., and Schulz, G. E. (2004) *Biochemistry* **43,** 11683–11690
14. Hallberg, B. M., Henriksson, G., Pettersson, G., and Divne, C. (2002) *J. Mol. Biol.* **315,** 421–434
15. Lario, P. I., Sampson, N., and Vrielink, A. (2003) *J. Mol. Biol.* **326,** 1635–1650
16. Ruiz-Dueñas, F. J., Ferreira, P., Martínez, M. J., and Martínez, A. T. (2006) *Protein Expr. Purif.* **45,** 191–199
17. Ferreira, P., Medina, M., Guillén, F., Martínez, M. J., van, Berkel, W. J. H., and Martínez, A. T. (2005) *Biochem. J.* **389,** 731–738
18. Ferreira, P., Ruiz-Dueñas, F. J., Martínez, M. J., van, Berkel, W. J., and Martínez, A. T. (2006) *FEBS J.* **273,** 4878–4888
19. Gibson, Q. H., Swoboda, B. E., and Massey, V. (1964) *J. Biol. Chem.* **239,** 3927–3934
20. Cleland, W. W. (1982) *Methods Enzymol.* **87,** 625–641
21. Gadda, G. (2003) *Biochim. Biophys. Acta* **1646,** 112–118
22. Fraaije, M. W., and van Berkel, W. J. H. (1997) *J. Biol. Chem.* **272,** 18111–18116
23. Roth, J. P., and Klinman, J. P. (2003) *Proc. Natl. Acad. Sci. U.S.A.* **100,** 62–67
24. Su, Q., and Klinman, J. P. (1999) *Biochemistry* **38,** 8572–8581
25. Ghanem, M., Fan, F., Francis, K., and Gadda, G. (2003) *Biochemistry* **42,** 15179–15188
26. Menon, V., Hsieh, C. T., and Fitzpatrick, P. F. (1995) *Bioorg. Chem.* **23,** 42–53
27. Gadda, G. (2003) *Biochim. Biophys. Acta* **1650,** 4–9
28. Ghanem, M., and Gadda, G. (2005) *Biochemistry* **44,** 893–904
29. Fan, F., Germann, M. W., and Gadda, G. (2006) *Biochemistry* **45,** 1979–1986
30. Romero, E., Ferreira, P., Martínez, A. T., and Martínez, M. J. (2009) *Biochim. Biophys. Acta* **1794,** 689–697
31. Rotsaert, F. A., Renganathan, V., and Gold, M. H. (2003) *Biochemistry* **42,** 4049–4056
32. Kass, I. J., and Sampson, N. S. (1998) *Biochemistry* **37,** 17990–18000
33. Lyubimov, A. Y., Lario, P. I., Moustafa, I., and Vrielink, A. (2006) *Nat. Chem. Biol.* **2,** 259–264
34. Li, H., Robertson, A. D., and Jensen, J. H. (2005) *Proteins* **61,** 704–721
35. Bright, H. J., and Gibson, Q. H. (1967) *J. Biol. Chem.* **242,** 994–1003
36. Kass, I. J., and Sampson, N. S. (1998) *Bioorg. Medicinal Chem. Lett.* **8,** 2663–2668
37. Fan, F., and Gadda, G. (2005) *J. Am. Chem. Soc.* **127,** 2067–2074
38. Gadda, G. (2008) *Biochemistry* **47,** 13745–13753
39. Hernández, A., Ferreira, P., Martínez, M. J., Romero, A., and Martínez, A. T. (2008) in *Flavins and Flavoproteins* (Frago, S., Gómez-Moreno, C., and Medina, M., eds) pp. 303–308, Prensas Universitarias, Zaragoza
40. Witt, S., Wohlfahrt, G., Schomburg, D., Hecht, H. J., and Kalisz, H. M. (2000) *Biochem. J.* **347,** 553–559
41. Müller, F., and Massey, V. (1969) *J. Biol. Chem.* **244,** 4007–4016
42. Massey, V., Müller, F., Feldberg, R., Schuman, M., Sullivan, P. A., Howell, L. G., Mayhew, S. G., Matthews, R. G., and Foust, G. P. (1969) *J. Biol. Chem.* **244,** 3999–4006
43. Massey, V., and Hemmerich, P. (1980) *Biochem. Soc. Trans.* **8,** 246–257
44. Massey, V. (1995) *FASEB J.* **9,** 473–475

SUPPLEMENTAL DATA

EXPERIMENTAL PROCEDURES

Two-substrate steady-state kinetic measurements

Reactions were carried out in a screw-cap cuvette where buffer was first equilibrated at the desired O_2 concentration (0.15, 0.32, 0.67 and 1.52 mM) by bubbling the corresponding O_2/N_2 gas mixture for 10-15 min. Assays were started by addition of the alcohol substrate (5-10 µL) and AAO at a final concentration of 0.03 µM, in a final volume of 1.5 mL.

Stopped-flow kinetic measurements

Reductive half-reactions were conducted under anaerobic conditions. Tonometers containing enzyme or substrate solutions were made anaerobic by successive evacuation and flushing with argon before being adapted to the stopped-flow syringes. These solutions also contained glucose (10 mM) and glucose oxidase (10 U) to ensure anaerobic conditions. Drive syringes in the apparatus were made anaerobic by sequentially passing dithionite and O_2-free buffer solutions before introducing the reactants (22). All concentrations mentioned are final ones obtained after mixing equal volumes of substrate and enzyme.

Solvent viscosity effect experiments

The solvent viscosity effect on steady-state parameters was measured at 25 ºC under atmospheric O_2 in 100 mM phosphate, pH 6, with different concentrations of glycerol. Relative viscosity values were taken from http://www.dow.com/glycerine/resources/table18.htm. Solvent viscosity effect on *p*-anisyl alcohol oxidation was determined from the ratio of the V_{max} and V_{max}/K_m values obtained in the absence of the viscosigen to those in the presence.

Data analysis

Data were fit using Sigmaplot (Systat. Sofware Inc. Richmond, CA, USA) and Pro-K softwares (Applied Photophysics Ltd.).
Kinetics parameters under atmospheric O_2 concentrations were determined by fitting initial reaction rates at different substrate concentration to the Michaelis-Menten equation for one substrate. Two-substrate steady-state kinetic observed rates were fit to **Eq. S1**, which describes a ternary complex mechanism;

$$\frac{v}{e} = \frac{k_{cat}SB}{K_m^B S + K_m^S B + SB + K_d K_m^B} \qquad \text{(Eq. S1)}$$

where, e represents the enzyme concentration, k_{cat} is the maximum turnover (catalytic constant; V_{max}, if saturating concentrations of both substrates are not used), S is the concentration of the alcohol substrate, B is the concentration of O_2, K_m^S and K_m^B are the Michaelis constants for S and B respectively, and K_d is the dissociation constant for the enzyme:substrate complex.
The pH dependence of V_{max} was determined by fitting initial rate data to **Eq. S2**

$$\log V_{max} = \log\left(\frac{C}{1+\frac{10^{-pK_a}}{10^{-pH}}}\right) \qquad \text{(Eq. S2)}$$

that describes a profile with a slope of -1 and a plateau at low pH. *C* is the pH-independent value of the kinetic parameter of interest, and pK_a is the pK_a of the residue whose protonation favors the reaction.
UV-visible spectral changes due to AAO-*p*-anisic acid complex formation were fit to **Eq. S3**

$$a = \frac{AI}{K_d + I} \qquad \text{(Eq. S3)}$$

where *a* and *A* are, respectively, the observed and maximal absorbance changes at the selected wavelength, and *I* is the inhibitor concentration.
Inhibition constants (K_i) were determined by nonlinear fitting of AAO activity inhibition to **Eq. S4**

$$\frac{v}{e} = \frac{k_{cat}S}{K_m\left(1+\frac{I}{K_i}\right)+S} \qquad \text{(Eq. S4)}$$

that describes a competitive inhibition pattern.
The K_i dependence on pH was fit to **Eq. S5**.

$$\log K_i = \log\left(\frac{C}{1+\frac{10^{-pH}}{10^{-pK_a}}}\right) \qquad \text{(Eq. S5)}$$

This equation describes a curve with a slope of +1 and a plateau at high pH, and pK_a is the pK_a of the residue whose protonation favors the inhibitor binding.
Spectral evolution analysis of reductive-half reactions was performed by global analysis and numerical integration methods. Accurate observed rate constants (k_{obs}) were obtained from single-wavelength traces recorded at 460 nm and fit into a standard double exponential decay, where k_{obs1} and k_{obs2} are the observed rate constants for the fast and slow phases, respectively. k_{obs1} values at different substrate concentrations were fit to either **Eqs. S6** or **S7**

$$k_{obs} = \frac{k_{red}S}{K_d + S} \qquad \text{(Eq. S6)}$$

$$k_{obs} = \frac{k_{red}S}{K_d + S} + k_{rev} \qquad \text{(Eq. S7)}$$

where k_{red} and k_{rev} are the limiting rates for the flavin reduction and the reverse reaction, respectively.
The observed ${}^{D}k_{cat}/K_m$ (in the sequential mechanism described by AAO) is given by **Eq. S8**

$${}^{D}\left(\frac{k_{cat}}{K_m}\right) = \frac{{}^{D}k_2 + C_f + {}^{D}EqC_r}{1 + C_f + C_r} \quad \text{(Eq S8)}$$

where ${}^{D}k_2$ is the intrinsic isotope effect for the cleavage of the *p*-anisyl alcohol CH bond, C_f and C_r are the forward and reverse commitments to catalysis, and ${}^{D}Eq$ is the equilibrium isotope effect which has a value of 1.24 for the conversion of an alcohol to an aldehyde (1).

1. Cleland, W. W. (1980) *Methods Enzymol.* **64,** 104-125

TABLE S1
Kinetic parameters (of steady and pre-steady states) **for AAO oxidation of *p*-anisyl alcohol and 2,4-hexadien-1-ol** (and its α-bideuterated analogs)
Steady and pre-steady state assays were performed in 100 mM phosphate, pH 6, at 24 and 12 ºC (respectively).

	Steady state[1]		Pre-steady state[2]	
	V_{max} (s^{-1})	V_{max}/K_m^S ($s^{-1}mM^{-1}$)	k_{red} (s^{-1})	$K_{d\ [AAO:S]}$ (μM)
p-Anisyl alcohol in H_2O	115 ± 2	3720 ± 157	112 ± 7	26 ± 6
p-Anisyl alcohol in D_2O	86 ± 3	3234 ± 281	79 ± 2	23 ± 3
[α-$^2H_2$]*p*-Anisyl alcohol in H_2O	21 ± 1	1002 ± 54	12 ± 1	23 ± 6
[α-$^2H_2$]*p*-Anisyl alcohol in D_2O	16 ± 1	608 ± 51	8 ± 1	7 ± 1
2,4-Hexadien-1-ol in H_2O	147 ± 3	1280 ± 88	138 ± 1	76 ± 5
2,4-Hexadien-1-ol in D_2O	117 ± 2	1017 ± 57	104 ± 1	87 ± 3
[α-$^2H_2$]2,4-Hexadien-1-ol in H_2O	26 ± 1	140 ± 13	15 ± 1	165 ± 12
[α-$^2H_2$]2,4-Hexadien-1-ol in D_2O	21 ± 1	84 ± 3	11 ± 1	124 ± 12

[1]Steady-state constants were determined at atmospheric O_2 concentration as described in the experimental section.
[2] Kinetic traces of AAO (FAD) reduction were fit to **Eq. S6**.

FIGURES

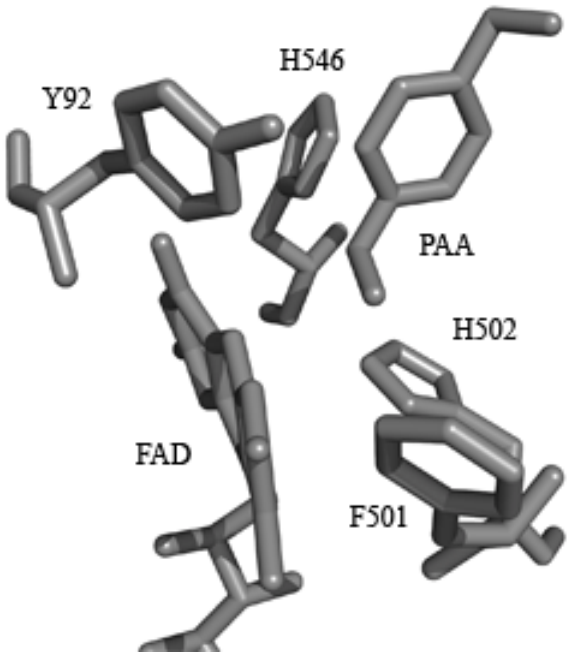

FIGURE 1S. **Active site of *P. eryngii* AAO.** The FAD cofactor, the two histidine and the two aromatic residues necessary for catalysis, as well as one docked *p*-anisyl alcohol (PAA) molecule (5) are shown in homology model for the AAO molecular structure (6).

5. Varela, E., Martínez, M. J., and Martínez, A. T. (2000) *Biochim. Biophys. Acta* **1481,** 202-208
6. Ferreira, P., Ruiz-Dueñas, F. J., Martínez, M. J., van Berkel, W. J. H., and Martínez, A. T. (2006) *FEBS J.* **273,** 4878-4888

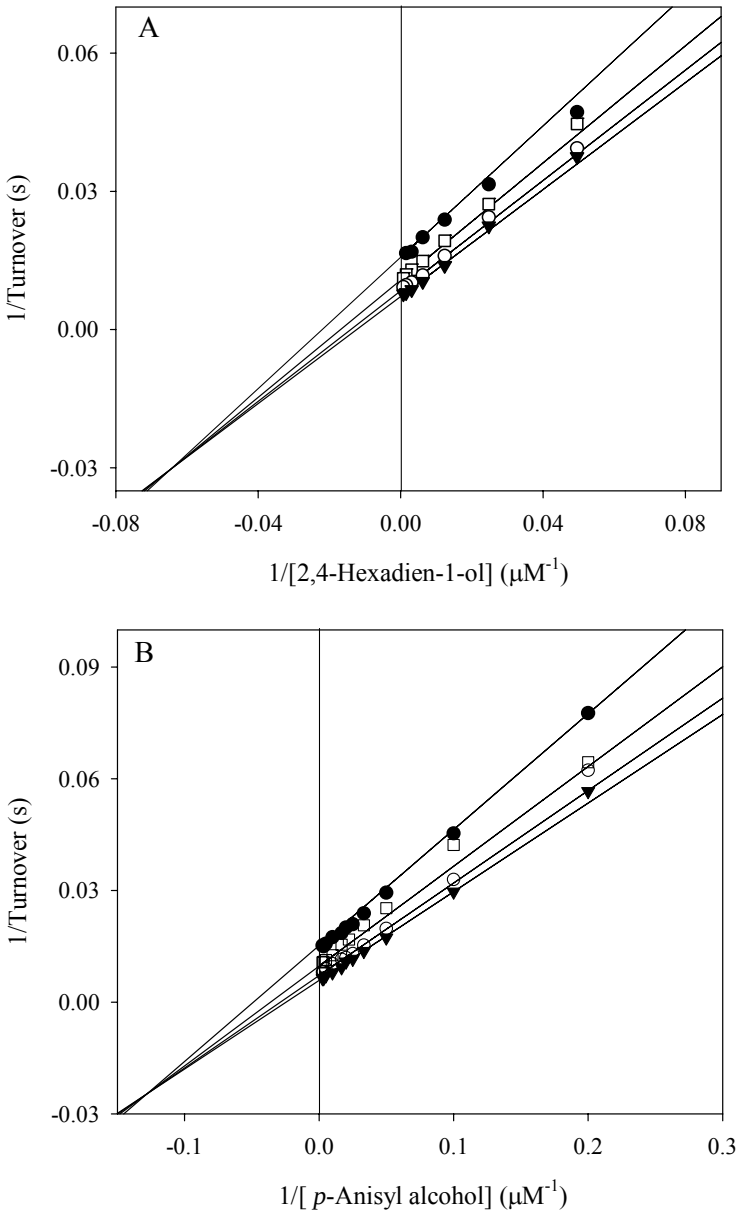

FIGURE 2S. **Double-reciprocal plot for AAO oxidation of *p*-anisyl alcohol (A) and 2,4-hexadien-1-ol (B).** Turnover numbers (micromoles of 2,4-hexadien-1-al or *p*-anisaldehyde formed by micromole of enzyme in one second) were measured in 100 mM phosphate, pH 6, at 12ºC, using different O_2 concentrations: 0.15 mM (●), 0.32 mM (□), 0.67 mM (O), 1.52 mM (▼). Lines are data fits to supplemental Eq. S1.

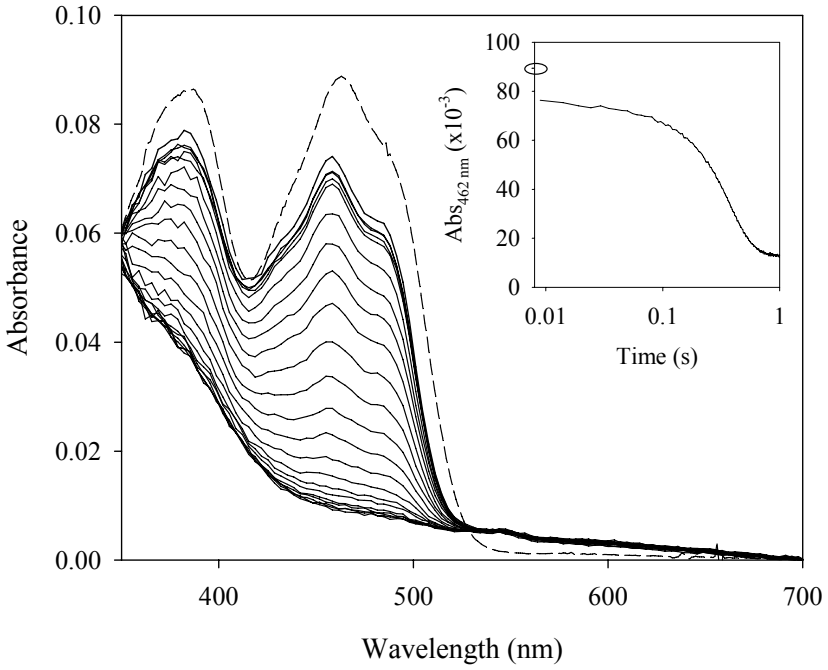

FIGURE 3S. **Time dependent spectral changes during AAO turnover with 2,4-hexadien-1-ol.** An aerobic solution of AAO (9 μM) was reacted in the stopped-flow instrument with 2 mM 2,4-hexadien-1-ol. The oxidized AAO spectrum before mixing is indicated by a dashed line, the first spectrum was recorded 0.009 s after mixing, in the 0.009-0.050 s range spectra are shown each 10 ms, and thereafter each 50 ms. The inset shows the course of the reaction monitored at 462 nm (logarithmic time scale). A closed circle indicates the initial absorbance of oxidized AAO. Measurements were carried out in 100 mM phosphate, pH 6, at 20 ºC.

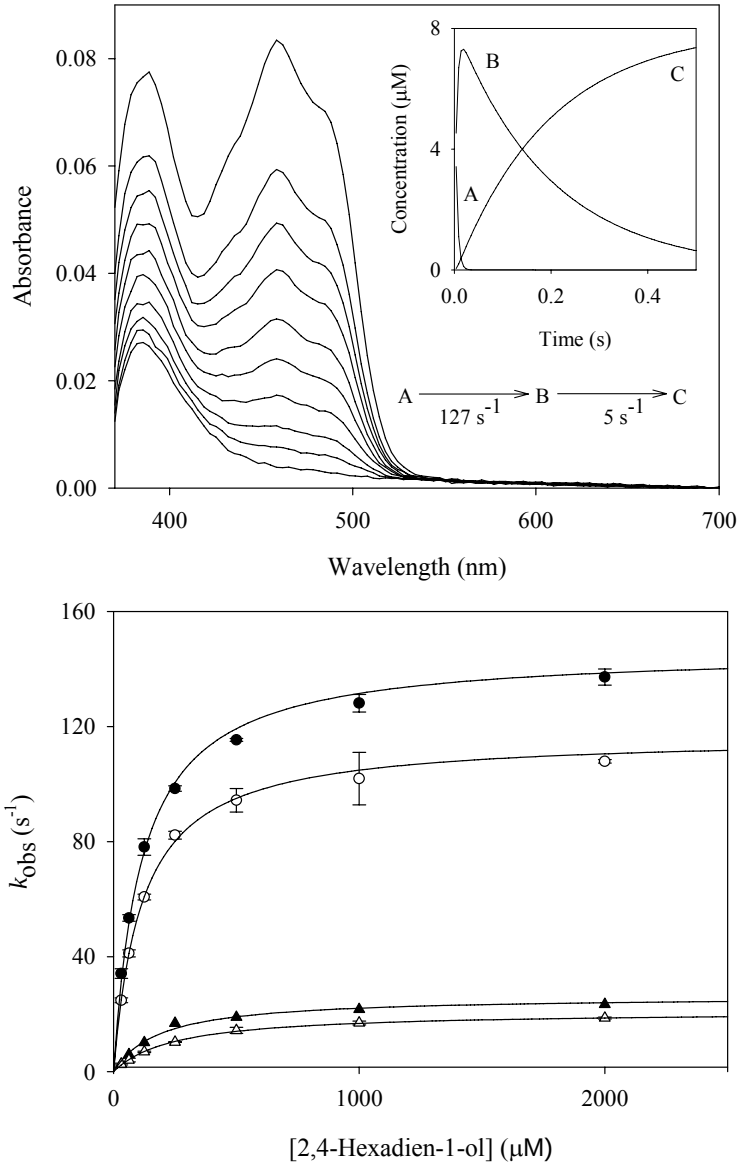

FIGURE 4S. **Reductive half-reaction of AAO with 2,4-hexadien-1-ol**. (Top) Spectral changes observed upon anaerobic mixing of 8 μM AAO with 700 μM 2,4-hexadien-1-ol. Spectra at 4, 8, 14, 29, 101, 168, 239, 316, 403 and 570 ms after mixing are shown. The inset shows the simulated concentration dependencies of the three spectral species obtained after globally fitting the experimental data to a three step model A→B→C. Species A, B and C are spectral species, reflecting a distribution of enzyme intermediates at a certain point along the reaction, and do not necessarily represent a single distinct enzyme intermediate. (Bottom) Dependence of the AAO reduction observed rates on the concentrations of 2,4-hexadien-1-ol (and its α-bideuterated analog) in water and deuterium oxide. Experiments performed with α-protiated substrates in water (●), α-protiated substrates in deuterium oxide (○), α-bideuterated substrates in water (▲) and α-bideuterated substrates in deuterium oxide (Δ). Data were fit to supplemental Eq. S6. Assays were carried out in a stopped-flow spectrophotometer at 12ºC.

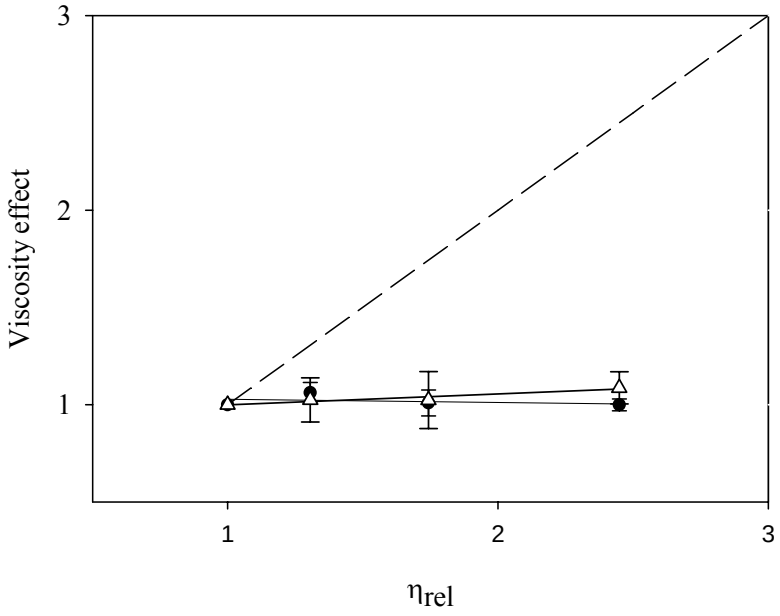

FIGURE 5S. **Effect of viscosity on AAO activity.** *V*max (●) and *V*max/*K*m (Δ) for *p*-anisyl alcohol oxidation by AAO under different viscosity conditions were estimated varying the substrate concentration in air-saturated reactions at 25ºC. Viscosity was increased with glycerol. Solid lines represent fits of the experimental data. The dashed line (with a slope of 1) indicates a fully diffusion-controlled reaction and η_{rel} is the relative viscosity.